

Hybrid-order topology of weak topological insulators

Sander H. Kooi,¹ Guido van Miert,¹ and Carmine Ortix^{1,2}

¹*Institute for Theoretical Physics, Center for Extreme Matter and Emergent Phenomena, Utrecht University, Princetonplein 5, 3584 CC Utrecht, the Netherlands*

²*Dipartimento di Fisica “E. R. Caianiello”, Università di Salerno, I-84084 Fisciano (Salerno), Italy*

 (Received 2 August 2019; revised 28 February 2020; accepted 7 July 2020; published 22 July 2020)

We consider weak topological insulators with a twofold rotation symmetry around their “dark” direction and show that these systems can be endowed with the topological crystalline structure of a higher-order topological insulator protected by rotation symmetry. These hybrid-order weak topological insulators display surface Dirac cones on all surfaces. Translational symmetry breaking perturbations gap the Dirac cones on the side surfaces leaving anomalous helical hinge modes behind. We also prove that the existence of this topological phase comes about due to a novel crystalline topological invariant of quantum spin-Hall insulators that can neither be revealed by symmetry indicators nor using Wilson loop invariants. Considering the minimal symmetry requirements, we anticipate that our findings could apply to a large number of weak topological insulators.

DOI: [10.1103/PhysRevB.102.041122](https://doi.org/10.1103/PhysRevB.102.041122)

Introduction. The essence of a free-fermion topological insulator is that it cannot be adiabatically deformed to a trivial atomic insulator, whose nature can be understood considering electrons as localized point particles. Put differently, topological insulators do not admit a representation in terms of exponentially localized Wannier functions (WFs). This obstruction to Wannier representability is, in turn, reflected in the presence of anomalous gapless boundary modes. Examples include the chiral (helical) edge modes in quantum (spin) Hall insulators [1–6], as well as the surface Dirac cones of three-dimensional topological insulators (TI) [7]. In crystalline systems with an additional set of spatial symmetries, additional topological phases can arise [8]. These topological crystalline insulators (TCI) cannot be represented in terms of WF respecting the spatial symmetries of the system, and feature, by the bulk-boundary correspondence, anomalous surface states violating a stronger version of the fermion doubling theorem [9] on surfaces that are left invariant under the protecting symmetry. Mirror Chern insulators [10,11], for instance, are characterized by the presence of gapless surface Dirac cones pinned to mirror planes. Similarly, higher-order topological insulators (HOTI) [12–15] feature anomalous gapless one-dimensional modes at the hinges connecting two surfaces related by the protecting crystalline symmetry [16].

The topologies related to the internal and spatial symmetries do not necessarily exclude each other and can also coexist. This occurs, for instance in different “dual” topological materials [17–20], which have the topological structure of both a weak TI and a mirror Chern insulator. Likewise, it has been recently proposed that certain topological superconductors can concomitantly feature both surface cones and Majorana hinge modes [21–23]. In all these systems, the topological crystalline structure can be diagnosed using the spatial symmetry content of the electronic bands [24–28] while the topology due to the internal symmetry is uniquely determined by the “tenfold-way” invariants [29–31]. There exist, however, certain topological crystalline phases that are

neither characterizable by symmetry indicators nor by the tenfold way [32]. In two-dimensional systems these phases have recently started to be classified [33].

The question that immediately arises is whether crystalline topologies without symmetry indicators can be embedded in a topological nontrivial insulating phase protected by an internal symmetry. In this work, we provide an affirmative answer by showing that two-dimensional topological insulators in the wallpaper group $p2$ —where time-reversal symmetry (TRS) guarantees the complete absence of symmetry indicators—can be characterized by a set of three crystalline topological \mathbb{Z}_2 indices. They correspond to two quantized partial Berry phases [34,35] and one additional novel topological index that cannot be diagnosed even from the Wilson loop. We subsequently use this new invariant to show that weak TIs possessing a twofold rotation symmetry around the $[\nu_1, \nu_2, \nu_3]$ direction, $\nu_{1,2,3}$ indicating the so-called weak topological indices [36], can be in a nontrivial topological crystalline phase. It is characterized by the presence of anomalous *unpinned* Dirac cones at the surfaces whose Miller indices (modulo 2) are identical to the weak topological indices, i.e., the so-called “dark” surfaces of weak TIs where surface Dirac cones protected by TRS are absent. This topological crystalline phase corresponds to a form of hybrid-order topology since the system can be switched to a HOTI with helical hinge modes using translational symmetry breaking perturbations.

Crystalline topological invariants in quantum spin-Hall insulators. We start out by developing a scheme that is able to capture the full crystalline topology of quantum spin-Hall insulators (QSHI) in systems with a twofold rotation symmetry C_2 . To do so, we first recall that for atomic insulating phases, the crystalline topology is fully determined by the gauge-invariant charge centers [9,33,37] of time-reversal symmetric Wannier functions that respect the symmetries of the crystal. The construction of such symmetric Kramers pairs of Wannier functions requires the construction of two time-reversed channels [5] of Bloch waves $|\Psi_n^{I,II}(q)\rangle$ that are separately

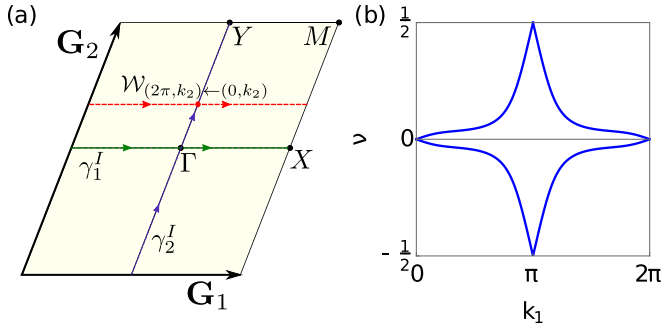


FIG. 1. (a) Schematic drawing of the Brillouin zone of C_2 symmetric crystal, spanned by reciprocal lattice vectors \mathbf{G}_1 and \mathbf{G}_2 . The partial polarizations are calculated along the green and blue line, and a typical Wilson loop contour is shown in red. (b) Wilson loop spectrum of a QSHI. The winding reflects the topological nontrivial nature of the insulating phase. The quantized value of the Wilson loop for $k_1 = 0$ corresponds to the quantized partial polarizations γ_2^I .

C_2 symmetric, where n is a band index running from one to $N_F/2$ and N_F the total number of occupied bands. The Bloch waves $|\Psi_n^{I,II}(q)\rangle$ need not be individual eigenstates of the Hamiltonian but are still basis states spanning the eigenspace corresponding to the N_F occupied bands. Importantly, the construction of symmetric Wannier functions requires a smooth, periodic, and symmetric gauge for the $|\Psi_n^{I,II}(q)\rangle$ Bloch waves. Since we want to study crystalline topology in non-Wannier representable QSHI, we relax these constraints on the gauge by demanding its smoothness, periodicity, and symmetry modulo a $\mathcal{U}(N_F/2) \otimes \mathcal{U}(N_F/2)$ gauge degree of freedom, with these two residual gauges acting in the two time-reversed and C_2 symmetric channels. In other words, we require a smooth, periodic, and symmetric set of projectors $\rho^{I(II)}(q) = \sum_n |\Psi_n^{I(II)}(q)\rangle \langle \Psi_n^{I(II)}(q)|$. In the Supplemental Material [38] we show how to construct such a gauge assuming for simplicity there are no degeneracies in the band structure other than those required by time reversal. Since within each sector we have not demanded a continuous gauge, it follows that the channels described by the Bloch waves $|\Psi_n^{I,II}(q)\rangle$ can be characterized by nonvanishing but opposite Chern numbers $C^{I,II}$. Furthermore, the twofold rotation symmetry endows the two channels with \mathbb{Z} indices that correspond to the multiplicities of the rotation eigenvalues $m_{\pm i}^I \equiv m_{\mp i}^{II}$ at the high-symmetry points in the Brillouin zone (BZ), i.e., $m = \Gamma, X, Y, M$ [see Fig. 1(a)].

We will now show that these integer crystalline indices and the Chern numbers of the channels can be used to construct four \mathbb{Z}_2 invariants that fully characterize the topology of C_2 and time-reversal symmetric insulators in two dimensions. Two \mathbb{Z}_2 invariants can be immediately identified in the quantized partial polarizations [34] on the C_2 symmetric lines of the BZ $k_{1,2} \equiv 0$. They correspond to the centers of charge of one-dimensional hybrid Wannier functions and are diagnosed [33] by the Wilson loop spectra $\nu(k_{1,2})$ [see Fig. 1(b)]. These quantized partial polarizations can be expressed in terms of the crystalline indices $m_{\pm i}^I$ as $\gamma_{1(2)}^I \equiv [\Gamma_i^I + X_i^I (Y_i^I)] \bmod 2$ (see the Supplemental Material [38] and Ref. [39]). The third \mathbb{Z}_2 invariant corresponds to the Fu-Kane-Mele invariant that characterizes QSHI and can be expressed

(see the Supplemental Material) in terms of the crystalline indices as $\nu_{\text{FKM}}^I = (\Gamma_i^I + X_i^I + M_i^I + Y_i^I) \bmod 2$. To define a fourth \mathbb{Z}_2 invariant, notice that the additional combination of eigenvalues $\nu_{1d}^I = (\Gamma_{-i}^I - X_{-i}^I - Y_{-i}^I + M_{-i}^I)/2 \bmod 2$ is linearly independent from the previously defined \mathbb{Z}_2 indices. For an atomic insulating phase, ν_{1d}^I corresponds to the parity of the time-reversed pairs of symmetric Wannier functions centered at the corner of the unit cell with coordinates $1d = \{1/2, 1/2\}$. The fact that in a QSHI the two time-reversed channels I, II are characterized by an odd Chern number immediately yields a semi-integer value $\nu_{1d}^I = \pm 1/2$. However, and this is key, we can still define a \mathbb{Z}_2 number reading

$$\gamma_3^I = \frac{1}{2} [C^I + (\Gamma_{-i}^I - X_{-i}^I - Y_{-i}^I + M_{-i}^I)] \bmod 2.$$

Being independent of the partial polarizations, this new integer cannot be diagnosed by the Wilson loop spectrum but still represents a well-defined and gauge-invariant crystalline topological number. In fact, γ_3^I is manifestly gauge invariant under intrachannel $\mathcal{U}(N_F/2)$ transformations since it is made out of a Chern number and the twofold rotation symmetry eigenvalues. Furthermore, γ_3^I is also invariant under interchannel gauge transformations, which correspond to the swapping of the channels ($I \leftrightarrow II$) for isolated pairs of bands. These transformations concomitantly change the sign of the Chern numbers of the channels and the multiplicities of the C_2 symmetry eigenvalues and therefore do not change γ_3^I . We have thus identified three gauge-invariant \mathbb{Z}_2 crystalline topological indices, which together with the Fu-Kane-Mele invariant yield a \mathbb{Z}_2^4 classification in agreement with a recent K theory study [40].

We finally emphasize that the gauge-invariant γ_3^I is different in nature from the ‘‘spin Chern numbers’’ existing in systems with a mirror symmetry \mathcal{M}_z . In this situation, the two time-reversed and C_2 symmetric channels I, II can be taken to be the spin eigenstates $|\uparrow\rangle, |\downarrow\rangle$, such that $C^I \equiv C^\uparrow$. However, this does not determine the value of γ_3^I , as the spin Chern number does not determine ν_{1d}^I . Thus one can find both $\gamma_3^I = 0, 1$ for the same spin Chern number.

Hybrid-order weak TIs. Next, we exploit the existence of the novel crystalline topology of γ_3^I in three-dimensional bulk crystals with a C_{2z} rotational symmetry. To do so, let us consider the three-dimensional Brillouin zone of our time-reversal invariant system as a collection of two-dimensional momentum cuts parametrized by the momentum k_z parallel to the twofold rotation axis. At the time-reversal invariant two-dimensional planes $k_z = 0, \pi$ we consider the system to be a topological nontrivial QSHI. As a result, the bulk three-dimensional crystal will be a three-dimensional topological insulator of the weak class. In principle, we could choose the two \mathbb{Z}_2 topological crystalline indices corresponding to the quantized partial polarization of the $k_z = 0, \pi$ QSHI to be different. This, however, would imply that in the triad of ‘‘weak’’ topological invariants [36] (ν_1, ν_2, ν_3) , ν_1 and/or ν_2 are different from zero. Hence, the three-dimensional system would feature an even number of surface Dirac cones protected by time reversal at the (001) and $(00\bar{1})$ surfaces that are left invariant under the C_{2z} rotation symmetry. As a result, any physical consequence of the crystalline topology cannot manifest itself: It would be completely obscured by the internal, time-reversal, symmetry topology.

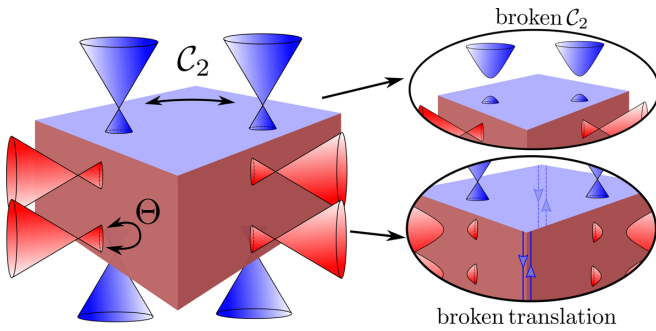


FIG. 2. Schematic of a hybrid-order weak topological insulator. At the top and bottom surfaces left invariant under the protecting C_{2z} symmetry a single pair of surface Dirac cones exist. On the side surfaces an even number of Dirac cones pinned to time-reversal invariant surface momenta are mandated by the weak topological invariants. When breaking C_2 symmetry, the topological crystalline surface Dirac cones at the top and bottom surfaces can be gapped out leaving these surfaces completely dark. By breaking the translational symmetry, i.e., doubling the unit cell, the time-reversal symmetry protected Dirac cones gap out, and the topological crystalline Dirac cones are then connected by helical hinge states.

However, we can choose the two \mathbb{Z}_2 topological crystalline invariants at the time-reversal invariant planes to be equal, thus constraining the weak invariants to be $(0, 0, 1)$. The time-reversal symmetric topology now guarantees the existence of an even number of massless Dirac cones appearing at time-reversal invariant (100) and (010) surface momenta (cf. Fig. 2), while the C_{2z} invariant (001) surfaces are completely gapped. A nontrivial crystalline topology, which can thus only arise from a difference in γ_3^I at the $k_z = 0, \pi$ planes, will then be in full force and lead to the appearance of a single pair of surface Dirac cones (cf. Fig. 2) at unpinned surface momenta related by the twofold rotation symmetry. This pair of surface Dirac cones realizes the rotational anomaly discussed in Ref. [9] and can be only removed by breaking the protecting C_{2z} and/or Θ symmetry (cf. Fig. 2). We point out that the existence of this rotation anomaly cannot be diagnosed by considering the flow of gauge-invariant Wannier centers between the $k_z = 0, \pi$ planes as in Ref. [9]. This is because at $k_z = 0, \pi$ our system is a topological insulator and therefore cannot be represented in terms of localized Wannier functions. The appearance of the unpinned Dirac surface cones is instead detected by considering the k_z -directed Wilson loop (see the Supplemental Material) in agreement with Ref. [41], although the stability of the surface Dirac cones cannot be inferred from the Wilson loop that consequently cannot be used to derive a “topological index.” We dub this new three-dimensional insulating phase a hybrid-order weak topological insulator: It is by itself a first-order topological insulator in $d = 3$ dimensions with $d - 1$ gapless boundary modes, but it can be switched using unit cell doublings in the \hat{z} direction, and thus without breaking any protecting symmetry, to a second-order topological crystalline insulator with anomalous gapless hinge modes (cf. Fig. 2) and C_2 rotation anomaly [9], and reminiscent of the surface cones one predicted to appear in $\alpha - \text{Bi}_4\text{Br}_4$ and a family of Zintl compounds [42,43].

Stacked Kane-Mele model. Having established the existence of the hybrid-order weak topological insulator, we

now present an explicit model based on stacked Kane-Mele systems realizing this phase. Let us consider a tight-binding model for spin-1/2 electrons on AA stacked honeycomb lattices. In momentum space the Bloch Hamiltonian can be written as:

$$\mathcal{H}(\mathbf{k}) = d_1(\mathbf{k})\tau_x \otimes s_0 + d_2(\mathbf{k})\tau_y \otimes s_0 + d_5(\mathbf{k})\tau_z \otimes s_z + d_4(\mathbf{k})\tau_z \otimes s_y, \quad (1)$$

where the τ_i 's and s_i 's are the Pauli matrices acting in sublattice and spin space, respectively. The first two terms in the Hamiltonian above correspond to intralayer spin-independent nearest-neighbor hopping processes, and the corresponding coefficients are $d_1(\mathbf{k}) = -t[1 + \cos x_1 + \cos x_2]$ and $d_2(\mathbf{k}) = -t[\sin x_1 + \sin x_2]$. Here we have introduced the hopping amplitude t while $x_{1,2} = \mathbf{k} \cdot \mathbf{a}_{1,2}$, $\mathbf{a}_{1,2}$ being the Bravais lattice vectors. The third term in the Hamiltonian Eq. (1) corresponds to spin-orbit interaction which involves intralayer spin-dependent second-neighbor hopping. We take the corresponding coefficient $d_5(\mathbf{k}) = 2t_2 \sin(x_1)$, with t_2 the hopping strength, thus explicitly breaking the threefold rotation symmetry. Finally, the last term in the Hamiltonian involves interlayer spin-dependent hopping amplitudes and the corresponding coefficient reads $d_4(\mathbf{k}) = -2t_3 \sin(k_z)$. We introduce this term to explicitly break the effective “in-plane” time-reversal symmetry [44] to allow for the possibility of a change of (crystalline) topology in the two time-reversal symmetric planes $k_z = 0, \pi$. Since the Hamiltonian Eq. (1) preserves bulk inversion symmetry, we can immediately obtain the strong and weak topological indices and thus obtain $(\nu_0; \nu_1, \nu_2, \nu_3) = (0; 0, 0, 1)$. In this form, however, Eq. (1) does not model a hybrid-order weak topological insulator: It can be adiabatically connected to a stack of uncoupled QSHI and consequently its (001) surface does not feature gapless modes. To endow the system with a nontrivial crystalline topology we instead modify the intralayer spin-orbit coupling as $d_5(\mathbf{k}) \rightarrow \cos(k_z)d_5(\mathbf{k})$. This modification keeps the strong and weak topological indices intact but changes the crystalline topology of the system. Note that also the inversion eigenvalues remain unchanged, thus implying that the hybrid-order phase cannot be diagnosed by inversion symmetry indicators.

To show this, we have computed the bulk band structure [see Fig. 3(a)] and the surface energy spectra [see Figs. 3(b), 3(c), and 3(d)] of this modified model by further accounting for an intralayer Rashba spin-orbit coupling term [45] of strength λ that explicitly breaks inversion symmetry. At the side surfaces we observe the conventional surface Dirac cones of a weak topological insulators [cf. Fig. 3(b)]. More importantly, diagonalization of the Hamiltonian with open boundary conditions along the stacking direction [cf. Fig. 3(c)] reveals the presence of two C_2 symmetry protected surface Dirac cones thus verifying that our model realizes a hybrid-order weak topological insulator. Note that the pairs of Dirac cones at the (001) and $(00\bar{1})$ surface are found at different surface momenta in agreement with the lack of inversion symmetry.

We have also verified that our model can be switched to a higher-order topological insulator by suitable translational symmetry breaking perturbations. Specifically we have introduced an interlayer staggered chemical potential of strength ϵ that provides the required doubling of the unit cell and

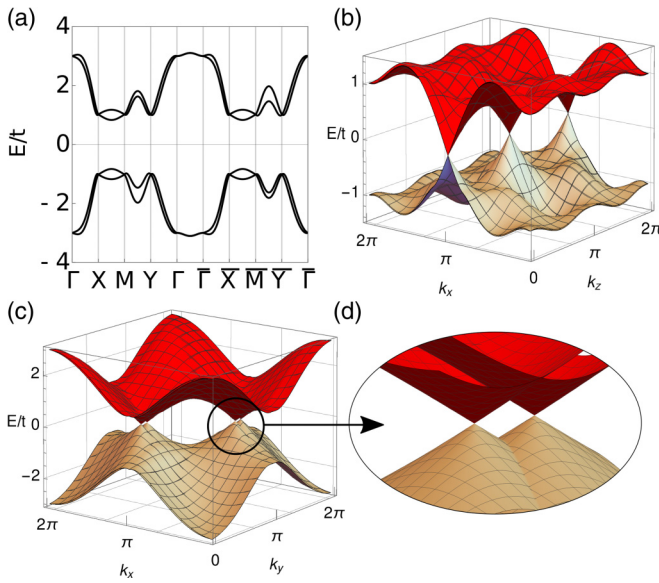


FIG. 3. (a) Bulk band structure of the stacked Kane-Mele model Eq. (1) by further accounting for a Rashba spin-orbit coupling term of strength $\lambda/t = 0.1$. The strength of the modified intralayer spin-orbit coupling term has been fixed to $t_2/t = 0.7$, whereas the interlayer spin-orbit coupling strength has been fixed to $t_3/t = 0.4$. (b) Energy spectrum in a slab geometry with open boundary conditions along the \hat{y} direction. The (010) and (0 $\bar{1}$ 0) surfaces exhibit an even number of Dirac cones pinned at time-reversal invariant surface momenta as required by the weak topological invariants. (c) Surface energy spectrum along the stacking \hat{z} direction. There are two pairs of surface Dirac cones localized at the (001) and the (00 $\bar{1}$) surface. The Dirac points are found at unpinned surface momenta related by the C_2 symmetry. The zoom-in (d) shows that the Dirac cones at opposite surface are located at different momenta due to the lack of inversion symmetry. All energies have been measured in unit of the hopping strength t .

further introduced an interlayer coupling in the enlarged unit cell of the form $-\delta\tau_z s_x$. Figure 4(a) shows the corresponding bulk band structure that is still characterized by a substantial gap. At the (010) [(0 $\bar{1}$ 0)] surface the time-reversal symmetry protected Dirac cones are gapped out [see Fig. 4(b)] while the twofold rotation symmetry-protected Dirac cones at the (001) [(00 $\bar{1}$)] surface are preserved [see Fig. 4(c)]. Notice that Dirac cone pairs localized at opposite surface are connected by helical hinge states [see Fig. 4(d)] as expected for a helical higher-order topological insulator protected by a twofold rotation symmetry.

Conclusions. To sum up, we have shown that weak topological insulators with an additional twofold rotation symmetry around the dark direction can feature a pair of Dirac cones on their dark surfaces, which are protected by the rotation symmetry. This hybrid-order weak topological

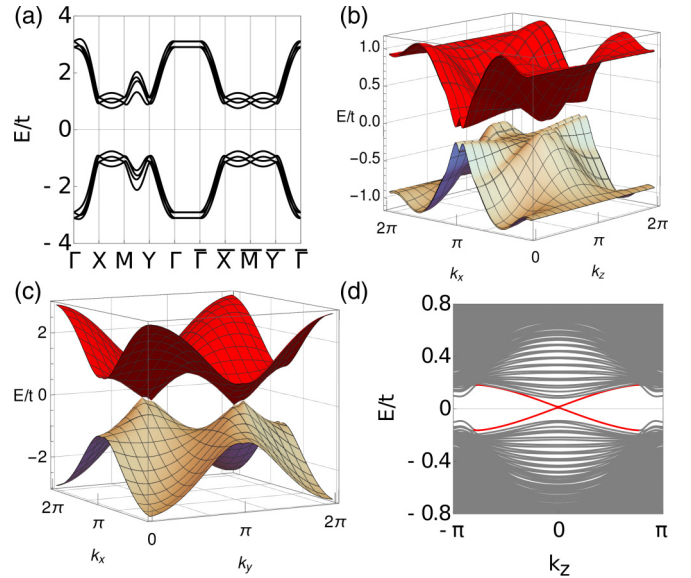


FIG. 4. (a) Bulk band structure of the stacked Kane-Mele model with a translational breaking perturbation. The parameter set is the same as in Fig. 3. Moreover the translational symmetry breaking parameters have been fixed to $\epsilon/t = 0.1$ and $\delta/t = 0.2$. (b) Surface energy spectrum showing the gapping of the time-reversal symmetry protected Dirac cones. (c) Surface energy spectrum along the stacking direction that still feature the C_2 -protected Dirac cones at unpinned surface momenta. (d) Energy spectrum in a ribbon geometry with periodic boundary conditions only along the stacking direction. Within the surface energy gap we find gapless anomalous helical hinge modes, colored in red.

insulator can be turned into a higher-order topological insulator with protected helical hinge modes by translational symmetry breaking perturbations. We have shown that the existence of such a topological phase comes about due to a third \mathbb{Z}_2 topological invariant characterizing quantum spin-Hall insulators in C_2 -symmetric crystals, that can be read off neither from symmetry indicators nor from the properties of the Wilson loop spectrum. Considering the minimal symmetry requirements and the fact that the C_2 protected surface Dirac cones appear at unpinned points in the surface Brillouin zone, we anticipate that our findings could apply to a large number of weak topological insulators.

Acknowledgments. C.O. acknowledges support from a VIDI grant (Project 680-47-543) financed by the Netherlands Organization for Scientific Research (NWO). This work is part of the research programme of the Foundation for Fundamental Research on Matter (FOM), which is part of the Netherlands Organization for Scientific Research (NWO). S.K. acknowledges support from a NWO-Graduate Program grant.

- [1] K. v. Klitzing, G. Dorda, and M. Pepper, *Phys. Rev. Lett.* **45**, 494 (1980).
- [2] D. J. Thouless, M. Kohmoto, M. P. Nightingale, and M. den Nijs, *Phys. Rev. Lett.* **49**, 405 (1982).
- [3] C. L. Kane and E. J. Mele, *Phys. Rev. Lett.* **95**, 226801 (2005).

- [4] C. L. Kane and E. J. Mele, *Phys. Rev. Lett.* **95**, 146802 (2005).
- [5] L. Fu and C. L. Kane, *Phys. Rev. B* **74**, 195312 (2006).
- [6] B. A. Bernevig, T. L. Hughes, and S.-C. Zhang, *Science* **314**, 1757 (2006).

- [7] L. Fu, C. L. Kane, and E. J. Mele, *Phys. Rev. Lett.* **98**, 106803 (2007).
- [8] L. Fu, *Phys. Rev. Lett.* **106**, 106802 (2011).
- [9] C. Fang and L. Fu, *Sci. Adv.* **5**, eaat2374 (2019).
- [10] T. H. Hsieh, H. Lin, J. Liu, W. Duan, A. Bansil, and L. Fu, *Nat. Commun.* **3**, 982 (2012).
- [11] T. H. Hsieh, J. Liu, and L. Fu, *Phys. Rev. B* **90**, 081112(R) (2014).
- [12] W. A. Benalcazar, B. A. Bernevig, and T. L. Hughes, *Science* **357**, 61 (2017).
- [13] F. Schindler, A. M. Cook, M. G. Vergniory, Z. Wang, S. S. Parkin, B. A. Bernevig, and T. Neupert, *Sci. Adv.* **4**, eaat0346 (2018).
- [14] F. Schindler, Z. Wang, M. G. Vergniory, A. M. Cook, A. Murani, S. Sengupta, A. Y. Kasumov, R. Deblock, S. Jeon, I. Drozdov *et al.*, *Nat. Phys.* **14**, 918 (2018).
- [15] G. van Miert and C. Ortix, *Phys. Rev. B* **98**, 081110(R) (2018).
- [16] S. H. Kooi, G. van Miert, and C. Ortix, *Phys. Rev. B* **98**, 245102 (2018).
- [17] M. Eschbach, M. Lanius, C. Niu, E. Młyńczak, P. Gospodarič, J. Kellner, P. Schüffelgen, M. Gehlmann, S. Döring, E. Neumann *et al.*, *Nat. Commun.* **8**, 14976 (2017).
- [18] N. Avraham, A. K. Nayak, A. Steinbok, A. Norris, H. Fu, Y. Sun, Y. Qi, L. Pan, A. Isaeva, A. Zeugner *et al.*, *Nat. Mater.* **19**, 610 (2020).
- [19] I. Rusinov, T. Menshchikova, A. Isaeva, S. Eremeev, Y. M. Koroteev, M. Vergniory, P. Echenique, and E. V. Chulkov, *Sci. Rep.* **6**, 20734 (2016).
- [20] J. I. Facio, S. K. Das, Y. Zhang, K. Koepnik, J. van den Brink, and I. C. Fulga, *Phys. Rev. Materials* **3**, 074202 (2019).
- [21] N. Bultinck, B. A. Bernevig, and M. P. Zaletel, *Phys. Rev. B* **99**, 125149 (2019).
- [22] S. A. A. Ghorashi, X. Hu, T. L. Hughes, and E. Rossi, *Phys. Rev. B* **100**, 020509(R) (2019).
- [23] S. A. A. Ghorashi, T. L. Hughes, and E. Rossi, [arXiv:1909.10536](https://arxiv.org/abs/1909.10536).
- [24] J. Zak, *Phys. Rev. B* **26**, 3010 (1982).
- [25] B. Bradlyn, L. Elcoro, J. Cano, M. G. Vergniory, Z. Wang, C. Felser, M. I. Aroyo, and B. A. Bernevig, *Nature (London)* **547**, 298 (2017).
- [26] J. Cano, B. Bradlyn, Z. Wang, L. Elcoro, M. G. Vergniory, C. Felser, M. I. Aroyo, and B. A. Bernevig, *Phys. Rev. Lett.* **120**, 266401 (2018).
- [27] E. Khalaf, H. C. Po, A. Vishwanath, and H. Watanabe, *Phys. Rev. X* **8**, 031070 (2018).
- [28] H. C. Po, A. Vishwanath, and H. Watanabe, *Nat. Commun.* **8**, 50 (2017).
- [29] A. Altland and M. R. Zirnbauer, *Phys. Rev. B* **55**, 1142 (1997).
- [30] A. Kitaev, *AIP Conf. Proc.* **1134**, 22 (2009).
- [31] J. Kruthoff, J. de Boer, J. van Wezel, C. L. Kane, and R.-J. Slager, *Phys. Rev. X* **7**, 041069 (2017).
- [32] Z.-D. Song, L. Elcoro, Y.-F. Xu, N. Regnault, and B. A. Bernevig, *Phys. Rev. X* **10**, 031001 (2020).
- [33] S. H. Kooi, G. van Miert, and C. Ortix, *Phys. Rev. B* **100**, 115160 (2019).
- [34] A. Lau, J. van den Brink, and C. Ortix, *Phys. Rev. B* **94**, 165164 (2016).
- [35] G. van Miert and C. Ortix, *Phys. Rev. B* **96**, 235130 (2017).
- [36] L. Fu and C. L. Kane, *Phys. Rev. B* **76**, 045302 (2007).
- [37] Z. Song, Z. Fang, and C. Fang, *Phys. Rev. Lett.* **119**, 246402 (2017).
- [38] See Supplemental Material at <http://link.aps.org/supplemental/10.1103/PhysRevB.102.041122> for more details.
- [39] T. L. Hughes, E. Prodan, and B. A. Bernevig, *Phys. Rev. B* **83**, 245132 (2011).
- [40] J. Kruthoff, J. de Boer, and J. van Wezel, *Phys. Rev. B* **100**, 075116 (2019).
- [41] L. Fidkowski, T. S. Jackson, and I. Klich, *Phys. Rev. Lett.* **107**, 036601 (2011).
- [42] C.-H. Hsu, X. Zhou, Q. Ma, N. Gedik, A. Bansil, V. M. Pereira, H. Lin, L. Fu, S.-Y. Xu, and T.-R. Chang, *2D Mater.* **6**, 031004 (2019).
- [43] T. Zhang, C. Yue, T. Zhang, S. Nie, Z. Wang, C. Fang, H. Weng, and Z. Fang, *Phys. Rev. Research* **1**, 012001 (2019).
- [44] A. Lau, C. Ortix, and J. van den Brink, *Phys. Rev. B* **91**, 085106 (2015).
- [45] The term is $[-1/2 + \cos(k_2) - \cos(k_1)]\tau_y \otimes s_x + [\sin(k_2) - \sin(k_1)/2]\tau_x \otimes s_x + [\sqrt{3}/2(\cos(k_1) - 1)]\tau_y \otimes \sigma_y + [\sin(k_1)\sqrt{3}/2]\tau_x \otimes s_y$.